

Water Fragmentation and Energy Loss by Carbon Ions at the Distal Region of the Bragg Peak

E. C. Montenegro,¹ M. B. Shah,² H. Luna,³ S. W. J. Scully,² A. L. F. de Barros,⁴ J. A. Wyer,² and J. Lecointre⁵

¹*Instituto de Física, Universidade Federal do Rio de Janeiro, Caixa Postal 68528 Rio de Janeiro, 21945-970, RJ, Brazil*

²*Department of Physics and Astronomy, Queen's University of Belfast, United Kingdom*

³*NCPST and School of Physical Science, Dublin City University, Republic of Ireland*

⁴*Departamento de Ensino Superior, Centro Federal de Educação Integrada Celso Suckow da Fonseca, Rio de Janeiro, Brazil*

⁵*Université Catholique de Louvain, Département de Physique, unité PAMO, Louvain-la-Neuve, Belgium*

(Received 16 July 2007; published 20 November 2007)

Time-of-flight mass spectrometry was used to investigate fragmentation and energy transfer processes in water by C ions at the distal part of the Bragg peak. Measurements of the positive ion fragments from ionization, electron capture, electron loss, transfer-loss and loss-ionization channels have allowed us for the first time (a) to obtain a quantitative determination of the energy lost by C ions in water and (b) to show that total water fragment ion production has a much flatter profile with projectile energy than would be expected if the water radical formation was assumed to follow the energy-loss profile obtained from available stopping power models.

DOI: 10.1103/PhysRevLett.99.213201

PACS numbers: 34.50.Gb, 34.50.Bw, 34.70.+e, 87.50.-a

The energy transfer and fragmentation patterns associated with intermediate-to-low-velocity heavy ion collisions in molecules is controlled by complex dynamics involving excitation, ionization, electron capture, and electron loss. This complexity means that applying simple inferences acquired in one system to another system could result in unacceptably large uncertainties. The extension of conceptual ideas and the execution of numerical simulations are consequently hindered due to the lack of experimental and theoretical guidance, and this affects important areas such as materials science, planetary atmospheres, radiation physics and medical physics. This is particularly true in the case of heavy ion collisions in water, where the amount of energy transferred and the sharing of energy between possible dynamic pathways is relatively unknown. Addressing this aspect is of particular importance due to the increasing popularity of C-ion based tumor therapies [1,2].

Intensity-modulated radiotherapy delivers high local doses to a defined treatment volume by selecting projectiles with energies such that the Bragg peak is centered within the tumor. These energies are determined by semi-empirical energy-loss calculations using the above-mentioned inferences [3,4] or by theoretical models which are currently rudimentary over the distal region of the Bragg peak [5]. As there are no reported experiments relating to energy transfer by low-energy C ions in water, even the uncertainties associated with these prescriptions cannot be realistically ascribed.

At the distal part of Bragg peak, the C beam consists predominantly of neutral and singly-charged components and both of these play major roles in energy transfers. It is clear that the widely used rule relating the stopping power of heavy ions with the stopping power of protons through an effective charge q , $S_{\text{HI}} = q^2 S_{\text{protons}}$ [6], fails if $q = 0$. Thus knowledge of ionization, electron capture and elec-

tron loss cross sections for a neutral beam in water is also mandatory to project beyond this point or accurate modeling of the Bragg peak distal region.

The general form for projectile energy loss for one active electron can be written as [7] (in a.u.):

$$\Delta E = \overbrace{I_p + \epsilon_i}^{\Delta E_{\text{loss}}} + \underbrace{I_T + E_p - 1/2u^2}_{\Delta E_{\text{ion}}} + \Delta E_{\text{exc}}, \quad (1)$$

where I_p and I_T are the ionization potentials of the projectile and of the target electron orbitals involved, respectively, ϵ_i is the kinetic energy of the ejected electron, E_p and $1/2 u^2$ are the final energy and the center of mass kinetic energy change of the captured electron, respectively, and Δ_{exc} is the excitation energy of the active electron.

ϵ_i and Δ_{exc} are small for C^0 and C^+ projectiles at low velocities, as is the energy loss in electron capture collisions when the parent ions remain intact. Thus, $\Delta E = \Delta E_0 + \epsilon_i + \Delta_{\text{exc}} \simeq \Delta E_0$ can be obtained, with small uncertainties, if the target orbitals involved in fragmentation are known. ΔE_0 is the part of ΔE which does not include ϵ_i or Δ_{exc} . The final collision products depend on which of the four water orbital electrons $2a_1$, $1b_2$, $3a_1$, and $1b_1$ is removed [8,9]. For instance, removal of the deep $2a_1$ and $1b_2$ electrons gives rise to fragmentation. Consequently, the energy lost by the projectile is closely related to the total fragmentation cross sections and these can be reliably used to establish a benchmark value for the electronic stopping power of C ions in water over the distal regions of the Bragg peak. It is shown in this Letter that this condition is indeed fulfilled. Furthermore, it is shown that the number of primary ions produced in water by C projectiles is almost flat from the distal part to the maximum of the Bragg peak.

Coincidence counting techniques have been used to uniquely measure the electron capture ($C^{q+} + H_2O \rightarrow C^{(q-1)+} + \Sigma H_2O^+$), the ionization ($\rightarrow C^{q+} + \Sigma H_2O^+ + e$) and the transfer-ionization processes ($\rightarrow C^{(q-1)+} + \Sigma H_2O^{2+} + e$), where $q = 0, 1$ and ΣH_2O^+ represents all the target channels. For C^0 projectiles, the loss-ionization ($\rightarrow C^+ + \Sigma H_2O^+ + 2e$) and the screening ($\rightarrow C^+ + H_2O + e$) channels were also measured. The main features of the crossed-beam experimental arrangement used in the present work have been described previously [10,11] and only a brief description is given here. A 1 mm diameter projectile beam crosses a 4 mm diameter target gas beam at 90° inside a high vacuum chamber. Two high transparency grids mounted on conical electrodes surrounded the crossed-beam region on either side and extract both the collision products of the target ions and the target electrons. The target gas beam was formed through effusion from a 2 mm diameter tube housed inside a separately pumped region. The extracted target ions were guided through a focusing lens system into a field free drift region before being detected by a stack of two multichannel plates (MCP). The target electrons extracted in the opposite direction were detected by a channeltron detector. A second channeltron detector placed downstream of the crossed-beam region, detected the charge changed projectile products separated from the main beam by electrostatic deflection. A time to amplitude converter (TAC), operated with start pulses supplied from the projectile detector or the target electron detector and stop pulses from the target ion MCP detector, provided time-of-flight (TOF) spectra for the capture and the ionization channels, respectively. The transfer-ionization channel was recorded in both spectra as this collision produces a fast projectile product as well as a target electron. In a second arrangement, the projectile beam was pulsed at a repetition rate of 10^5 Hz and a width of 150 ns and the TAC start pulses were supplied directly from the beam pulsing unit. The TOF spectrometer then recorded all the target ion products from the capture and ionization collisions including transfer ionization. In this arrangement transfer ionization is only recorded once. Subtraction of the pulsed spectra from the summed spectra obtained separately in coincidence with the projectile products, and with the target electrons gives the transfer ionization contributions and thus the pure electron capture and the pure ionization contributions. A flight distance of 240 mm was used to provide well-resolved spectra of the close lying O^+ , OH^+ , and H_2O^+ target group. The H^+ ions carrying a major portion of the dissociation energy diverge rapidly and required a distance of 30 mm for complete collection. The measurements were normalized using a proton beam.

Figure 1 shows the measured cross sections for H_2O ion products by C^0 and C^+ projectiles. The C^0 measurements include ionization, electron capture and loss-ionization channels, while the C^+ include ionization and electron

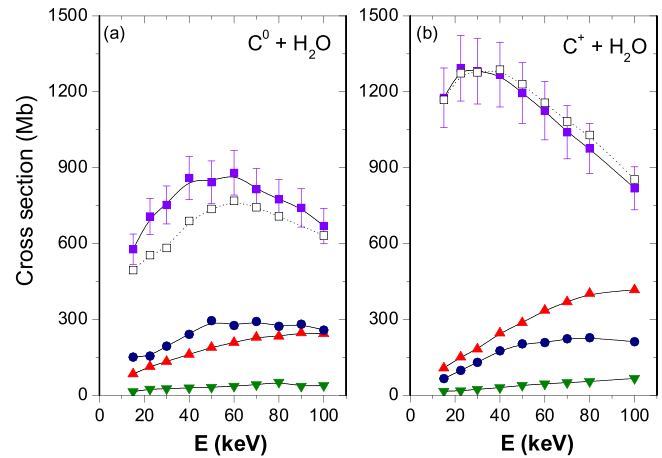


FIG. 1 (color online). Cross sections for positive ion production by C^0 (a) and C^+ (b) in water. Squares, H_2O^+ , circles, OH^+ , up triangles H^+ , down triangles, O^+ . Open squares corresponds to *total* positive ion production by ionization in the case of (a) and by electron capture in the case of (b). Lines drawn are to guide the eye. Error bars are included only for H_2O^+ for clarity.

capture. As seen in Fig. 1, ionization dominates ion production for C^0 projectiles and electron capture for C^+ projectiles.

For both the projectiles, the H_2O^+ cation from the weakly bound $1b_1$ and $3a_1$ levels is the main product ion channel in ionization and electron capture collisions and the O^+ from the strongly bound $2a_1$ molecular orbital [9] is the smallest channel, indicating clearly that these collisions strongly favor small amounts of energy transfer.

Figure 1 shows that collisions involving C^0 are very important and should not be ignored in energy-loss calculations as has been done in the past. As shown in Fig. 2, C^0 is a substantial component of the C beam at the distal part

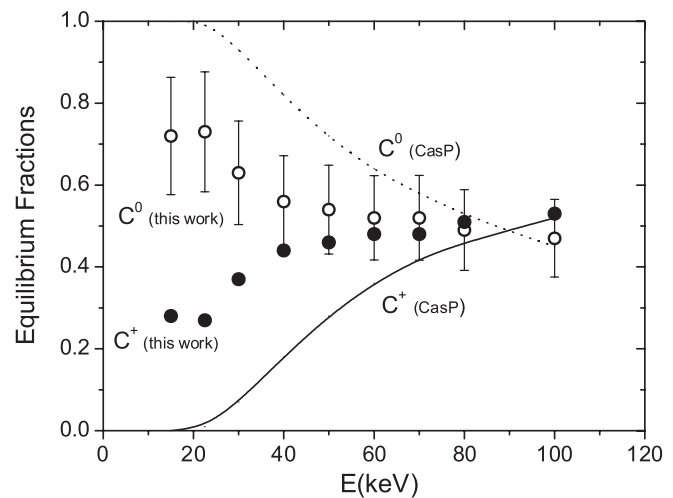


FIG. 2. Equilibrium charge-state fractions for C beam in water. Open and closed circles are from this work. Lines indicated as CasP are from Ref. [5].

of the Bragg peak. The equilibrium fractions, (f_0) and (f_1) of C^0 and C^+ , respectively, shown over the energies relevant to this region are calculated from the ratio $f_1/f_0 = \sigma_{\text{loss}}^{C^0}/\sigma_{\text{cap}}^{C^+}$ [12] using cross sections taken from our measurements. Also shown in Fig. 2 are the calculated values from Ref. [5]. The fractions of Ref. [5] are in good agreement with ours at 100 keV but diverge rapidly at lower collision energies.

Each of our measured collision channels involve a ΔE energy loss. This can be assessed by considering which of the four water orbital electron is removed during the collision. For both electron capture and ionization, the average binding energy can be taken as $I_T = I_A = (I_{1b_1} + I_{3a_1})/2$. An upper limit for the energy transferred in electron capture by C^+ is $\Delta E_{\text{cap}} = I_A - 1/2 u^2 - 1/n^2$, with the $n = 3$ final state being inferred from recent classical-trajectory Monte Carlo method calculations of low-velocity, multiply-charged ions in water [13]. In the case of ionization, as noted, the ejected electron energy is strongly peaked at zero kinetic energy and first-order estimates for the energy transfer [14] give $\Delta E_{\text{ion}} = (11/10)I_A$ for the ejection of p electrons in the low-velocity limit. The screening contribution of the C^0 electron loss—where the water molecule remains in the ground state [15]—can be viewed as an ionization in the projectile frame and $\Delta E_{\text{screen}} = (11/10)I_p = 11.7$ eV. The C^0 loss-ionization is a two-electron removal channel and gives important contributions to electron loss. $\Delta E_{\text{loss-ion}} = (11/10)(I_{AA} + I_p)$, where I_{AA} is the average energy of all but the $1a_1$ molecular orbitals. I_{AA} reflects the measured distribution of fragments for this channel better than I_A . The transfer-ionization cross sections for C^+ ions are less than 8% of the total fragment production. The energy loss for this process is $\Delta E_{\text{transfer-ion}} = \Delta E_{\text{cap}} + 2.8(11/10)I_A$. Here the binding energy of the second removed electron is accounted for through the factor 2.8 [16].

The rate of energy loss with distance traveled in liquid water can then be given for each channel by $(dE/dx)_{\text{channel}} = n \Delta E_{\text{channel}} \sigma_{\text{channel}}$, where n is the number density of liquid water. The total energy loss dE/dx due to all the channels is shown in Fig. 3 together with that for each of the above individual channels in the inset (A). The charge-state equilibrium fractions of Fig. 2 were used to calculate the weighted contributions to both these quantities.

The experimentally derived energy-loss values around the Bragg peak maximum, where C^{3+} forms the majority of ions in the beam, are also shown using the C^{3+} measurements of Ref. [10] together with the q^2 scaled contributions from ionization and the scaled law of Ref. [17] contributions for capture, to include the q^{2+} and q^{4+} fractions present in the beam around this region. In the liquid phase, the contribution from the drag forces induced by the traveling projectile, is estimated to be ≈ 0.3 eV/nm through the Firsov model [18] at 15 keV, i.e., less than

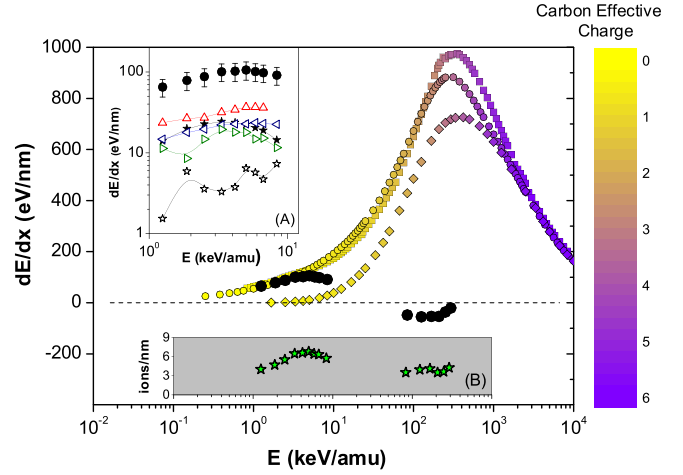


FIG. 3 (color online). Total energy-loss rate of the C beam passing through water. Symbols: large black closed circles—values derived from present experimental work (15 to 100 keV) and that of Ref. [10] (1500 to 3500 keV); closed squares—calculations from Ref. [3]; closed circles—calculations from Ref. [4]; closed diamonds—calculations from Ref. [5]. Symbols representing the calculations are gray coded (color online) according to the equilibrium charge-state (vertical bar on right) found at various C energies across the Bragg peak (Ref. [5]). Inset (A) shows the energy loss calculated for our measured ionization (up-side triangles), electron capture (closed stars), loss-ionization (left side triangles), screening (right-side triangles), and transfer-ionization (open stars) cross sections and their summed values (closed circles). Inset (B) shows the number of ions/length obtained from our measurements.

0.5% of our reported value, and is neglected. We estimate that the combined uncertainties of adopted values for the average energy of ejected electron in ionization, electron loss and transfer-ionization channels, and the final state of the captured electron are within 20% for energies below 30 keV. Including the experimental uncertainties, $dE/dx = 65 \pm 16$ eV/nm at the collision energy of 15 keV. Figure 3 also shows the calculated total energy loss values of Refs. [3–5] using stopping power models.

Inset (A) of Fig. 3 shows that ionization, electron capture, and projectile electron loss (loss ionization + screening) contribute on an equal footing at the distal low-energy end of the Bragg peak. The good agreement between the total energy-loss values of Refs. [3,4] with the present ones at energies below 40 keV should be considered fortuitous as Ref. [3] uses an effective charge based on the theory by Brandt and Kitagawa [6,19] which is valid only for high velocities and does not include electron capture or electron loss, while Ref. [4] is based on a fit of ratios between empirical stopping data of heavy ions and alpha particles, but no previous data exist in this energy region for either C or He in water. The calculations of Ref. [5] do not include explicit electron capture contributions and, as seen in Fig. 3, they underestimate the present total energy loss below 100 keV.

The present energy-loss values in Fig. 3 are derived by considering $\Delta E \approx \Delta E_0$. This assumption is not true for energies well above 100 keV. At the Bragg peak maximum the contribution from ΔE_0 gives a *projectile energy gain*, due to contributions from electron capture [7,20], and the energy of the ejected electrons ϵ_i for C^{q+} ions, with $q \approx 3$, must be of the order of 200 eV to account for the projectile energy loss estimated by the various models. This conclusion agrees with the observation of large energy transfers, mostly carried away by the ejected electrons, in ≈ 1 MeV/amu C^{q+} , O^{q+} and F^{q+} ($q = 5-9$) ions colliding with Ne [7,21,22] and He [20]. These results lead to the conclusion that the ion production rate to which free-radical production relates directly, suggests that the water related damage around the Bragg peak is much lower than appears from the energy-loss perspective. Our measurements give a direct indication of the actual number of primary free radicals produced and, as seen in inset (B) of Fig. 3, these remain almost constant over a substantial portion of the Bragg peak. Indeed, in both low-energy distal and the Bragg peak maxima regions, the number of primary ions produced is $N_{\text{ion}}/\text{length} = n \sum \sigma_{\text{channel}} \approx 4-8$ ions/nm. The number of ions produced by 200 eV electrons estimated from ionization [9] and energy loss [23] by electrons in water gives $\approx 8-10$ ions/nm. This means that the ratio between the number of ions produced at the Bragg peak maxima (300 keV/amu) and at the distal part (3 keV/amu) is ≈ 2 , while the ratio of the stopping powers is ≈ 10 . Thus even when the added contributions from energetic secondary electrons is accounted for, the ion production falls far short of that suggested by the Bragg peak derived from high energy stopping power theories. In other words, ion production is not as sharply localized as suggested by Bragg peak energy-loss profiles. In fact, primary ion production is far from being localized and is actually relatively uniform at a region where the ions come to rest. This finding could have important implications in treatment planning of C-ion therapy, mainly when tumors are located closer to critical organs such as optical nerves [24]. The flatter damage profile may also require future dosage calculations currently based on stopping power models to be reconsidered.

Support of the EPSRC (UK) and from Brazilian Agencies CNPq, CAPES and FAPERJ is acknowledged. E. C. M. thanks the IRCEP at Queen's University of Belfast for the hospitality. J. A. W. thanks the Department of Education, Northern Ireland for additional support. Authors gratefully acknowledge the valuable comments by P. L. Grande.

- [1] D. Schulz-Ertner and H. Tsujii, J. Clin. Oncol. **25**, 953 (2007).
- [2] D. Schulz-Ertner *et al.*, Int. J. Radiat. Oncol. Biol. Phys. **67**, 171 (2007).
- [3] J. F. Ziegler, Nucl. Instrum. Methods Phys. Res., Sect. B **219**, 1027 (2004); SRIM 2003 version 26 available from: <http://www.srim.org>.
- [4] H. Paul and A. Schinner, At. Data Nucl. Data Tables **85**, 377 (2003); MSTAR version 3 available from: <http://www.exphys.unilinz.ac.at/Stopping/>.
- [5] P. L. Grande and G. Schiwietz, Nucl. Instrum. Methods Phys. Res., Sect. B **195**, 55 (2002); CasP, version 3.1 available from: <http://www.hmi.de/people/schiwietz/casp.html>.
- [6] A. F. Lifschitz and N. R. Arista, Phys. Rev. A **69**, 012902 (2004).
- [7] M. A. Abdallah *et al.*, Phys. Rev. Lett. **85**, 278 (2000).
- [8] W. Hwang, Y.-K. Kim, and M. E. Rudd, J. Chem. Phys. **104**, 2956 (1996).
- [9] E. C. Montenegro, S. W. J. Scully, J. A. Wyer, V. Senthil, and M. B. Shah, J. Electron Spectrosc. Relat. Phenom. **155**, 81 (2007).
- [10] H. Luna and E. C. Montenegro, Phys. Rev. Lett. **94**, 043201 (2005).
- [11] H. Luna, C. McGrath, M. B. Shah, R. E. Johnson, M. Liu, C. J. Latimer, and E. C. Montenegro, Astrophys. J. **628**, 1086 (2005).
- [12] J. C. Armstrong, J. V. Mullendore, H. R. Harris, and J. B. Marion, Proc. Phys. Soc. London **86**, 1283 (1965).
- [13] S. Otranto, R. E. Olson, and P. Beiersdorfer, J. Phys. B **40**, 1755 (2007).
- [14] E. C. Montenegro and A. G. de Pinho, J. Phys. B **15**, L275 (1982).
- [15] E. C. Montenegro, W. E. Meyerhof, and J. H. McGuire, Adv. At. Mol. Opt. Phys. **34**, 249 (1994).
- [16] J. P. Richardson, J. H. D. Eland, P. G. Fournier, and D. L. Cooper, J. Chem. Phys. **84**, 3189 (1986).
- [17] H. Knudsen, H. K. Haugen, and P. Hvelplund, Phys. Rev. A **23**, 597 (1981).
- [18] E. C. Montenegro, S. A. Cruz, and C. Vargas-Aburto, Phys. Lett. A **92**, 195 (1982).
- [19] W. Brandt and M. Kitagawa, Phys. Rev. B **25**, 5631 (1982).
- [20] W. Wu, K. L. Wong, C. L. Cocke, J. P. Giese, and E. C. Montenegro, Phys. Rev. A **51**, 3718 (1995).
- [21] V. Frohne, S. Cheng, R. Ali, M. Raphaelian, C. L. Cocke, and R. E. Olson, Phys. Rev. Lett. **71**, 696 (1993).
- [22] H. Schöne *et al.*, Phys. Rev. A **51**, 324 (1995).
- [23] H. Iskef, J. W. Cunningham, and D. E. Watt, Phys. Med. Biol. **28**, 535 (1983).
- [24] A. Hasegawa, J.-E. Mizoe, A. Mizota, and H. Tsujii, Int. J. Radiat. Oncol. Biol. Phys. **64**, 396 (2006).